New and Improved Photometric Metallicity Estimator for SDSS, v1.4

Željko Ivezić[1], Timothy C. Beers[2], Young Sun Lee[2], Deokkeun An[3], Branimir Sesar[4], Mario Jurić[5], Sarah Loebman[1], Constance M. Rockosi[6], Donald P. Schneider[7] who else, Heather M., Jennifer J., ???

Received ______________________; accepted ______________________

[1]Department of Astronomy, University of Washington, Box 351580, Seattle, WA 98195

[2]Dept. of Physics & Astronomy and JINA: Joint Institute for Nuclear Astrophysics, Michigan State University, East Lansing, MI 48824

[3]Ewha Womans University, 11-1 Daehyun-Dong Seodaemun-Gu, Seoul 120-750, Korea

[4]California Institute of Technology, Pasadena, CA 91125

[5]Hubble Fellow, Harvard College Observatory, 60 Garden St., Cambridge, MA 02138

[6]University of California–Santa Cruz, 1156 High St., Santa Cruz, CA 95060

[7]Department of Astronomy and Astrophysics, The Pennsylvania State University, University Park, PA 16802

ABSTRACT

We present a new calibration of SDSS photometric metallicity estimator, based on a spectroscopic sample of ∼95,000 F and G stars from Data Release 8. We also improve statistical treatment and correct for metallicity bias due to large $u - g$ errors of faint stars. The proposed procedure estimates metallicity using the $u - g$ and $g - r$ colors, as well as the $u - g$ error, and can be easily implemented with provided tabular data. The method and results presented here supercede previously published calibrations based on Data Releases 6 and 7.

Subject headings: methods: data analysis — stars: statistics

1. INTRODUCTION

Stellar metallicity, together with effective temperature and surface gravity, is one of the three main parameters that affect observed properties of stars. The knowledge of stellar metallicity is crucial for accurate estimates of distances using photometric parallax relation, see Jurić et al. (2008) and Ivezić et al. (2008b, hereafter I08), and the variation of metallicity distribution within the Galaxy provides constraints for the theories of galaxy formation and evolution (e.g., Majewski 1993; Freeman & Bland-Hawthorn 2002; Helmi 2008; Majewski 2010; and references therein).

The most accurate measurements of stellar metallicity are based on spectroscopic observations. Despite the recent progress in the availability of stellar spectra (e.g., SDSS has recently made publicly available over XXX,000 stellar spectra as a part of its Data Release 8; RAVE may provide up to a million spectra over the next few years), the number of stars detected in imaging surveys is vastly larger. In addition to generally providing better sky and depth coverage than spectroscopic surveys, an advantage that is becoming even more important with the advent of deep optical surveys such as Pan-STARRS (Kaiser et al. 2002), Dark Energy Survey (Flaugher 2008) and LSST (Ivezić et al. 2008a), imaging surveys obtain essentially complete flux-limited samples of stars.

Motivated by these advantages of imaging surveys, and aided by the large sample of SDSS stars with spectroscopic metallicity (Beers et al. 2006; Lee et al. 2008a; Lee et al. 2008b), I08 adapted the traditional UV-excess based $\delta(U-B)_{0.6}$ method (Wallerstein 1962; Sandage 1969) to the SDSS photometric system. The method relies on the fact that the metallicity of blue main sequence (F and G type) stars is correlated with the difference between the star's $u-g$ color and the $u-g$ color which would be measured for a metal-rich star with the same $g-r$ color. The physical origin of this correlation is the increasing absorption of UV photons by metallic lines as the metallicity increases (at a constant effective temperature, that is, at a constant $g - r$ color). The method developed by I08 can be easily applied using a polynomial expression that maps the measured $u - g$ and $g - r$ colors to the metallicity scale. Due to changes in the calibration of SDSS spectroscopic metallicity between Data Releases 6 and 7, Bond et al. (2010) provided an updated set of polynomial coefficients.

The calibration of SDSS spectroscopic metallicity changed again between Data Releases 7 and 8 (though changes are much smaller than between Data Releases 6 and 7, see § 2.2), which motivates this work. An even stronger motivation comes from a recent discovery that photometric metallicity estimator is biased for faint stars with large measurement errors for the $u - g$ color (Lee et al. 2011). In the next Section, we describe a statistical method that incorporates the information about $u - g$ measurement errors and accounts for this bias. Our results are discussed in Section 3.

2. ANALYSIS

We begin by summarizing data selection criteria and spectroscopic metallicity differences between Data Releases (DR) 7 and 8. We follow by an illustration of the statistical origin of photometric metallicity bias based on a toy model, and describe Bayesian and heuristic methods that account for this bias.

2.1. Data Selection

The spectroscopic sample used here for the calibration of photometric metallicity is selected in the first step using the selection criteria listed in Section 2.3.1 in I08. Starting with 320,000 stars that have DR8 SSPP parameters, we select 168,000 stars with $0.2 < g - r < 0.6$ and $g < 19.5$. With additional constraints that distance (computed as described in I08) is in the 1-10 kpc range, galactic latitude $b > 30°$, 3<log(g)<6, and that spectroscopic metallicity is in the range $-3 <$ [Fe/H] < 0.5, we obtain the final sample of 95,000 stars (∼60% more than for DR 7 sample).

2.2. Comparison of DR8 and DR7 Spectroscopic [Fe/H]

The differences between spectroscopic metallicity values distributed with SDSS DR 7 and 8 are of the order 0.1 dex. Figure 1 summarizes the behavior of these differences, which are due to software updates, as a function of colors and metallicity itself. The changes between DR7 and 8 are significantly smaller than changes between DR6 and DR7 (compare to figure A.1 in Bond et al. 2010). Hence, the application of polynomial expressions for estimating photometric metallicity from Bond et al. (2010) to DR8 catalogs will result in systematic errors of about 0.1 dex (comparable to the intrinsic precision of the method). However, the bias at the faint end, described in the next section, will remain.

2.3. Metallicity Bias Due to u-g Color Errors

In order to illustrate the impact of photometric errors on photometric metallicity estimates, we use a toy model motivated by observations. Model values are generated by drawing [Fe/H] from a flat distribution in the range -3 to 0, and computing colors from

$$y = 0.84 + 0.34 \times 10^{(0.45\,x)} \tag{1}$$

where $x =$ [Fe/H] and $y = (u - g)$. These values are then randomized using Gaussian distributions with $\sigma = 0.1$ (both for [Fe/H] and $u - g$) to simulate observational scatter due to measurement errors. The adopted functional form is motivated by the fact that the

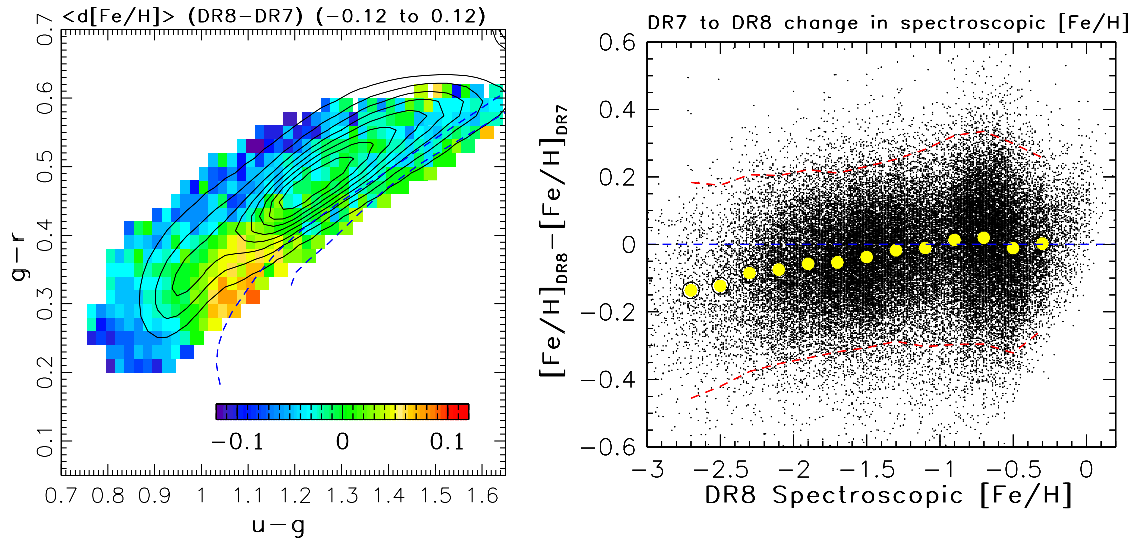

Fig. 1.— Summary of the differences between SDSS spectroscopic-metallicity values distributed with Data Releases (DR) 7 and 8. The left panel shows the median difference between the DR8 and DR7 values for $0.02{\times}0.02$ mag^2 bins in the $g-r$ vs. $u-g$ color-color diagram, color-coded according to the legend shown in the panel. The largest differences are only $\sim$0.1 dex, with a root-mean-square scatter of 0.04 dex. The distribution of stars with $r < 20$ and at high Galactic latitudes is shown as linearly spaced contours. The two dashed lines correspond to globular clusters NGC 2420 and M67, with metallicities -0.37 and 0.0, respectively, and are added for completeness (see § 2.7). The right panel shows the difference in metallicities as a function of the new DR8 values. Individual stars are shown as small dots, and the binned median values of the difference are shown as large circles. The two dashed lines mark the $\pm 2\sigma$ envelope around the medians, where σ is the root-mean-square scatter estimated from the interquartile range (0.1-0.15 dex, due to software updates). The median differences are larger than 0.1 dex only at the very low-metallicity end ([Fe/H]< -2.5).

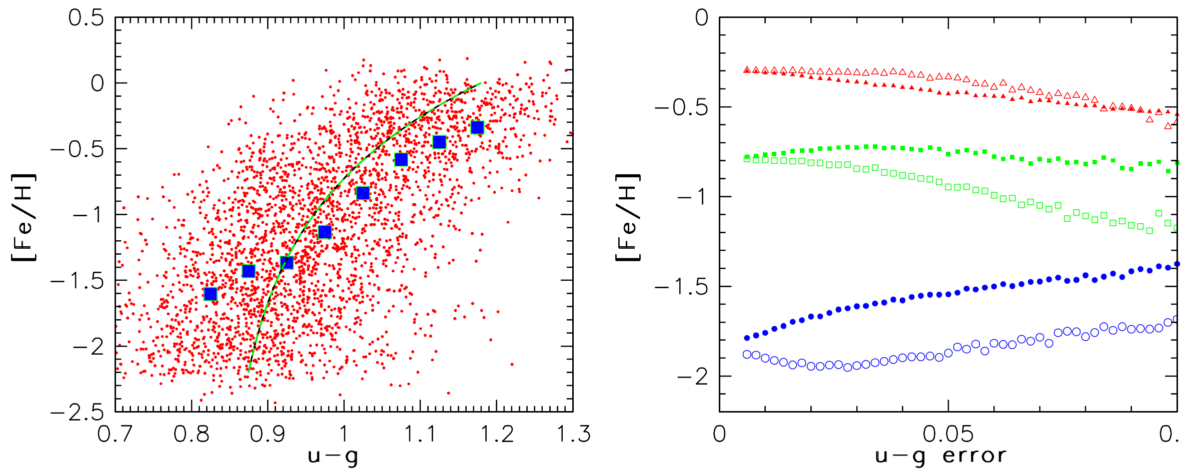

Fig. 2.— A toy model for illustrating a bias in photometric metallicity estimator due to large $u-g$ color errors. About 4,000 small dots in the left panel are generated as described in § 2.3. The dashed line represents eq. 1. The large symbols are the median values of [Fe/H] in bins of $u-g$ color. The curves in the right panel show the median [Fe/H] as a function of assumed $u-g$ errors (Gaussian distributions; the left panel is generated with $\sigma = 0.1$ mag), for three values of the $u-g$ color: 0.89 (circles), 0.99 (squares) and 1.09 (triangles). Open symbols correspond to the case with uniform [Fe/H] distribution (shown in the left panel), and closed symbols to the case where [Fe/H] is made of two equal-size concatenated Gaussian distributions centered on [Fe/H] = −1.5 and [Fe/H] = −0.5, and with σ equal to 0.3 dex and 0.2 dex, respectively.

ultraviolet flux is absorbed by metallic lines according to the Beer's law[1], and coefficients are determined by fitting data for stars with $g-r \sim 0.3$.

The simulated sample is shown in the left panel in fig. 2. Its behavior vividly demonstrates that adopting a median value (or any other average statistic) of spectroscopic [Fe/H] in bins of $u-g$ color as photometric metallicity estimator fails miserably when $u-g$

[1]This law is not named after the second author.

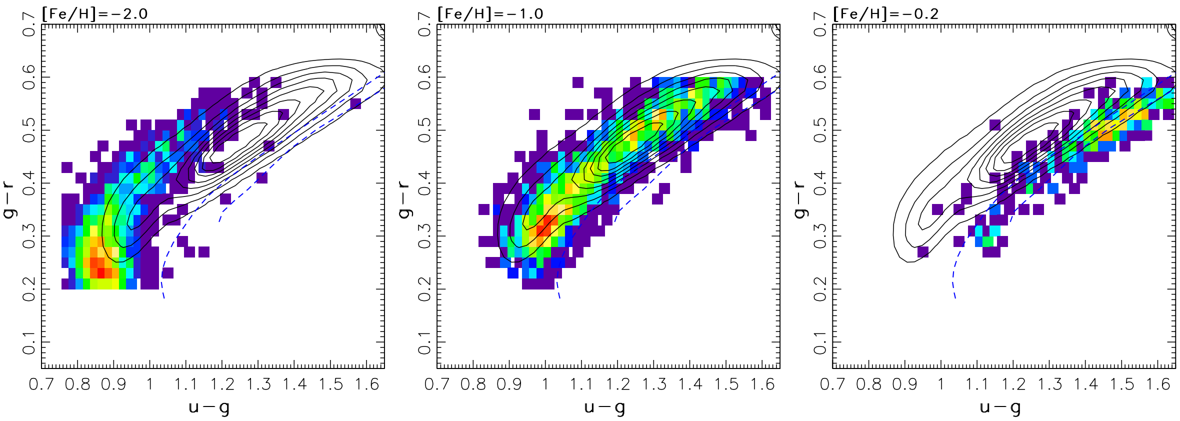

Fig. 3.— The probability distribution $p(ug, gr|[\mathrm{Fe/H}])$, discussed in § 2.4. The maps shown for different values of [Fe/H] (−2.0, −1.0 and −0.2) are essentially (renormalized) counts of stars selected from 0.1 dex wide bins centered on given values of [Fe/H]. The color-coded maps are displayed on a logarithmic scale, with contours and dashed lines having the same meaning as in fig. 1.

errors are not negligible (compared to the relevant dynamic range – this is why $u - g$ errors are more important here than errors in spectroscopic [Fe/H]). In particular, the resulting median [Fe/H] values are biased high at low [Fe/H] (blue $u - g$) and biased low at high [Fe/H] (red $u - g$).

The severity of this bias depends on errors. The right panel in fig. 2 shows the bias as a function of assumed $u-g$ errors for three different values of true $u-g$. Note that metallicity bias can be both positive and negative. As expected, there is no bias for vanishing errors. The bias also depends on the details of the underlying (true) [Fe/H] distribution (see figure caption), and it is especially strong when "measured" values of $u - g$ are bluer than the bluest possible $u - g$ color in the zero-noise case ($u - g < 0.84$, see eq. 1). Statistical treatment of this effect is described in next two sections.

2.4. Practical Difficulties with Bayesian Treatment

The problem outlined in the preceding section can be treated using standard Bayesian approach, with the posterior probability distribution of [Fe/H] (the probability of [Fe/H] *given* the measured values of $ug = u - g$ and $gr = g - r$) computed via

$$p([\mathrm{Fe/H}]\,|\,ug, gr) \propto p(ug, gr\,|\,[\mathrm{Fe/H}])\,p([\mathrm{Fe/H}]). \tag{2}$$

The probability distribution $p(ug, gr|[\mathrm{Fe/H}])$ can be thought of as the (normalized) distribution of stars selected from a narrow [Fe/H] bin in the $g - r$ vs. $u - g$ color-color diagram. Examples of $p(ug, gr|[\mathrm{Fe/H}])$ for three different values of [Fe/H] determined using the stellar sample described in section 2.1 are shown in fig. 3. In the one-dimensional case discussed in preceding section (without dependence on the $g - r$ color), $p(ug|[\mathrm{Fe/H}])$ corresponds to the $u - g$ distribution in a horizontal narrow slice centered on the corresponding value of [Fe/H]. That is, in the toy model discussed above, this distribution is given by a Gaussian with $\sigma = 0.1$ mag, and centered on values given by eq. 1.

With $p([\mathrm{Fe/H}]|ug, gr)$ available, it is straightforward to compute the expectation value (and any other statistic) for photometric metallicity as

$$< [\mathrm{Fe/H}] >= \int [\mathrm{Fe/H}]\,p([\mathrm{Fe/H}]\,|\,ug, gr)\,d[\mathrm{Fe/H}]. \tag{3}$$

Here, $< [\mathrm{Fe/H}] >$ is a function of input $u - g$ and $g - r$, but we supress explicit dependence for notational simplicity. This function is shown in the left panel in fig. 4. The distribution of $< [\mathrm{Fe/H}] >$ differs from the median [Fe/H] employed by I08 and B10, as shown in the right panel.

It is noteworthy that $p([\mathrm{Fe/H}]|ug, gr)$ does not follow a Gaussian distribution. Indeed, $p([\mathrm{Fe/H}]|ug)$ for $u - g < 0.84$ in the toy model increases without bound towards low values of [Fe/H] and it is only the prior, $p([\mathrm{Fe/H}])$, that prevents the integral in eq. 3 from diverging. The $<$ [Fe/H] $>$ map shown in fig. 4 was computed using a uniform prior for $-3 <$ [Fe/H] < 1, and 0 outside this range.

While in principle the Bayesian treatment provides sound theoretical framework, its implementation is difficult in this case due to heteroscedastic errors (errors are not constant and increase towards the faint end). As can be seen in fig. 4, even when the full sample is considered, $p([\mathrm{Fe/H}]|ug, gr)$ can be fairly noisy because the sample if subdivided in narrow [Fe/H] bins. To properly account for heteroscedastic errors, such maps would not only have to be produced for bins of [Fe/H], but for bins of the $u-g$ color errors, $ugErr$, as well (the impact of $g-r$ errors is negligible compared to that of $u-g$ errors). That is, $p([\mathrm{Fe/H}]|ug, gr)$ would have to be generalized to $p([\mathrm{Fe/H}]|ug, gr, ugErr)$. With this additional binning in the fourth direction, the resulting maps become too noisy due to frequent small number of stars per pixel (many pixels with less than 10 stars). Instead, we resort to a heuristic method described in the next section.

2.5. Heuristic Treatment

We seek a metod for incorporating information about the $u-g$ errors, in addition to $u-g$ and $g-r$ measurements, to avoid a bias in estimated photometric metallicity. Instead of further subdividing subsamples from pixels in the $g-r$ vs. $u-g$ color plane into two-dimensional bins of [Fe/H] and $u-g$ errors, we choose to fit [Fe/H] as a linear function of $u-g$ errors in each pixel (note that the method used by I08 and B10 simply adopts the median [Fe/H] value for each pixel). This ansatz results in less stringent requirements for the sample size (by one to two orders of magnitude), at the expense of forcing a given functional form. The choice of a linear function is arbitrary and motivated by simplicity, as well as by the behavior shown in the right panel in fig. 2. We have also fit a quadratic function, but the results did not substantially improve over those presented below.

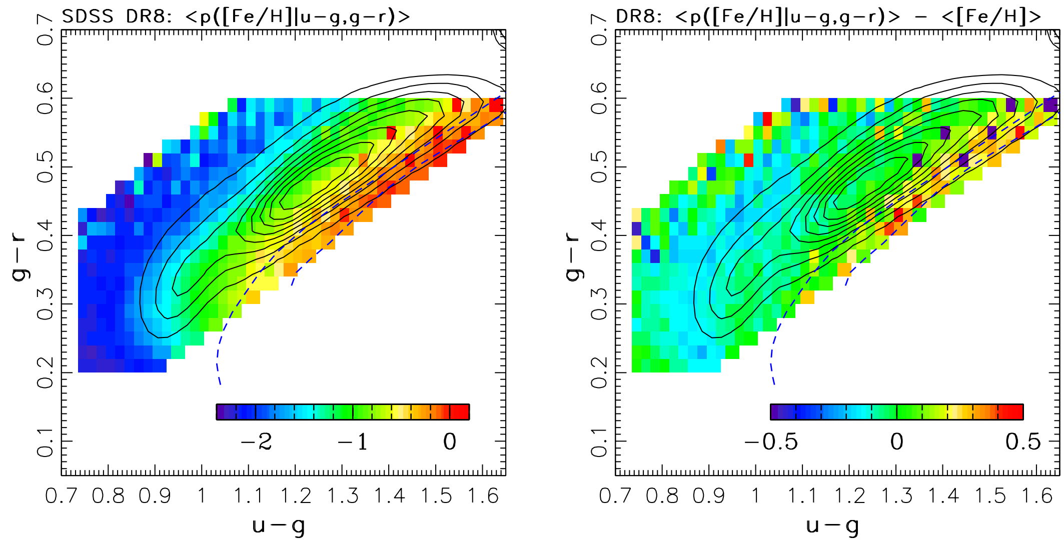

Fig. 4.— The left panel shows the expectation value for metallicity computed using eq. 3, color-coded according to the legend. Contours and dashed lines have the same meaning as in fig. 1. The right panel shows the difference between this map and the median values of [Fe/H] in each pixel, color-coded according to the legend. The median value of the difference for all pixels is −0.05 dex, with root-mean-square scatter of 0.13 dex. The difference is about 0.4 dex at the metal-rich end. The two maps are not the same because the Bayesian map in the left panel accounts for the bias discussed in § 2.3.

The result of this procedure are two maps, shown in fig. 5, rather than a single map as in the case of adopting the median [Fe/H]. With these maps, $A(ug, gr)$ and $B(ug, gr)$, the photometric metallicity, $[\mathrm{Fe/H}]_{ph}$ is estimated as

$$[\mathrm{Fe/H}]_{ph} = A(ug, gr) \times ugErr + B(ug, gr) \tag{4}$$

where ug, gr and $ugErr$ are the measured values for a given star. The methods developed by I08 and B10 are equivalent to adopting the median [Fe/H] for map B, and setting $A = 0$.

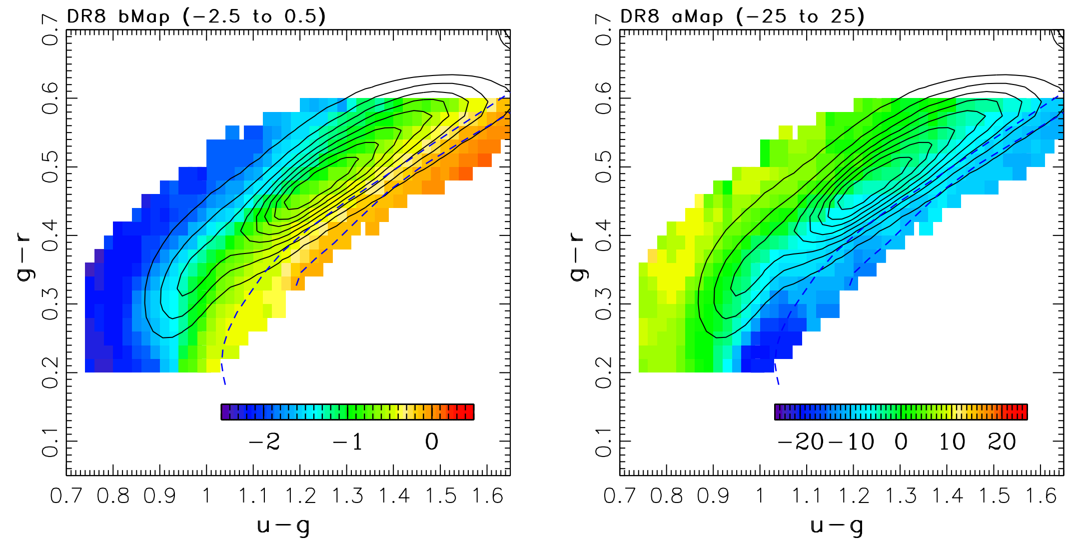

Fig. 5.— The panels show the maps $B(ug, gr)$ (left) and $A(ug, gr)$ (right) defined in eq. 4, color-coded according to legends. Contours and dashed lines have the same meaning as in fig. 1. The $B(ug, gr)$ map shown in the left panel corresponds to the expected [Fe/H] for stars with perfectly measured $u - g$ colors. The bias due to finite $u - g$ errors, discussed in § 2.3, is assumed to be a linear function of $u-g$ errors, with the coefficients of proportionality given by the $A(ug, gr)$ map shown in the middle panel. The map in the right panel shows the median difference between spectroscopic and revised photometric metallicities for ∼95,000 stars from SDSS DR 8. The median of all pixel values is zero, and the root-mean-square scatter is 0.057 dex.

The structure discernible in the $A(ug, gr)$ map implies that the metallicity bias due to $u - g$ cannot be corrected for using a single correction coefficient (independent of colors). The $B(ug, gr)$ map and the Bayesian map shown in the left panel in fig. 4 are fairly similar; however, they are not equal because the latter corresponds to some "effective" average value of $u - g$ errors for the sample used in calibration. While fitting the [Fe/H] vs. $ugErr$

relationship in each pixel, we have also computed the median residual and root-mean-square scatter for the best-fit. Their statistical behavior indicates that the choice of linear fitting function is satisfactory. An indication that fits are stable across independent pixels is the smoothness of resulting maps. A few outlying pixels, located mostly along the map edges were smoothed out using a 3×3 pixel large median filter. The root-mean-square scatter of the difference between smoothed and "raw" values is only 0.01 dex for B map, and the median value of the metallicity noise contribution due to the smoothing of A map is 0.05 dex.

It is noteworthy that the dependence of photometric metallicity estimator on prior p([Fe/H]), discussed in § 2.4, is "hidden" in this method because here we directly determine the expectation value $<$ [Fe/H] $>$ (see eq. 3) via eq. 4. In other words, the distribution of the calibration (training) sample in the three-dimensional (ug, gr, $ugErr$) space is automatically encoded in $A(ug, gr)$ and $B(ug, gr)$ maps. If, for example, a single (ug, gr) pixel contained an overwhelming majority of all stars in the training sample, photometric metallicity in *all* bins "within the reach" of their $ugErr$ error scatter would be strongly biased towards the corresponding [Fe/H] value (that is, the smaller number of stars that "arrived" from other pixels would be "outvoted"). Hence, when fitting the [Fe/H] vs. $ugErr$ relationship in each pixel, individual stars should be weighted by the inverse of their selection probability (we assumed uniform weights). Given that the selection function for SDSS spectroscopic sample is very complex (see the bottom right panel in fig. 3 from I08), this sensitivity of our results to p([Fe/H]) causes concern and we quantify it below using a mock stellar sample.

2.6. A Recipe for Estimating Photometric Metallicity

Following I08 and B10, we attempted to derive convenient polynomial fits to maps shown in fig. 5. We were unable to obtain fits with residuals smaller than about 0.1-0.2 dex (varying across the $g-r$ vs. $u-g$ plane) due to more fine structure in these maps than in the map of median [Fe/H]. Since the functional forms employed by I08 and B10 are already cumbersome, we opted against even more complex forms and decided to provide the resulting two maps in tabular form (see Table 1). For given $u-g$ and $g-r$ colors, the appropriate values of A and B maps can be simply found by searching for the nearest pixel (which can be done fast with an appropriate indexing scheme). This approach has an added benefit that the sample does not have to be carefully pre-selected using colors – stars that are further away than ∼0.03 mag from any 0.02×0.02 mag^2 pixel should be rejected from further analysis.

In summary, photometric metallicity can be estimated by following these steps:

- The method is valid for stars with $0.2 < g-r < 0.6$ and the $u-g$ range populated by the maps (corresponding SDSS sample is dominated by main sequence F and G stars).
- The calibration with respect to $u-g$ errors is valid for $ugErr < 0.1$, roughly corresponding to SDSS stars with $r < 20$.
- For given $u-g$ and $g-r$ measurements, get the corresponding values of A and B maps by searching for the nearest pixel. The method is only applicable to stars whose measured colors place them at most 0.03 mag from the nearest pixel.
- Compute the expectation value for [Fe/H] using eq. 4. Its systematic error is shown in the left panel in fig. 6, and typical random errors vary from ∼0.2 dex at the high-metallicity end to ∼0.3 dex at the low-metallicity end (see the middle panel in

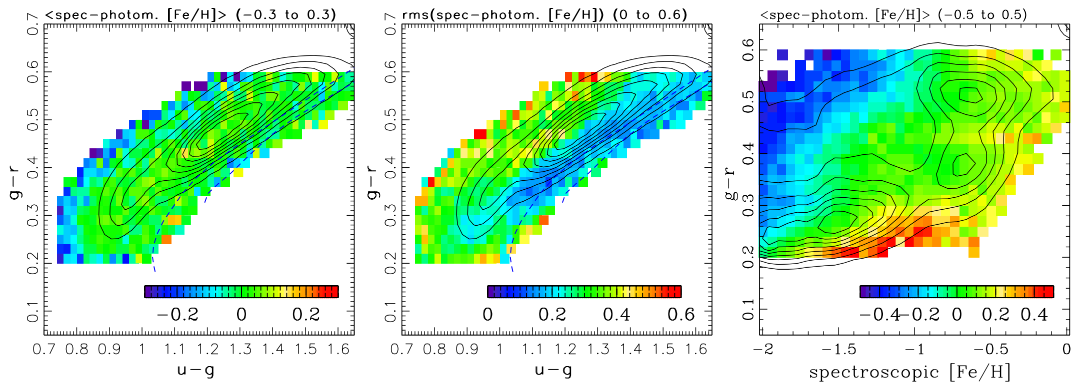

Fig. 6.— The map in the left panel shows the median difference between spectroscopic and revised photometric metallicities for ∼95,000 stars from SDSS DR 8, as a function of $u-g$ and $g-r$ colors. The median of all pixel values is zero, and the root-mean-square scatter is 0.057 dex. The middle panel shows the root-mean-scatter in each pixel (note that the scatter is lower for high-metallicity stars with red $u-g$ and $g-r$ colors). The right panel shows the median difference between spectroscopic and photometric metallicities as a function of $g-r$ color and spectroscopic metallicity. The linearly spaced contours show the distribution of stars in the calibration sample. Note that the median discrepancies are small for well-populated regions.

fig. 6), for stars from the calibration sample. The dependence of random errors on magnitude is discussed in §2.3.3 in I08.

2.7. Testing

We test the revised photometric metallicity estimators using similar methods as I08 and B10. The median difference between spectroscopic and photometric metallicity as a function of $u-g$ and $g-r$ colors is shown in the left panel in fig. 6. The median of all pixel values is zero, and the root-mean-square scatter is 0.057 dex. The scatter is a bit smaller than 0.07 dex obtained by B10, probably due to avoidance of polynomial fitting, which also contributes to the final errors. The root-mean-square scatter per bin is shown in the middle panel in fig. 6, and it varies from $\sim$0.15 dex for high-metallicity stars to $\sim$0.3 dex for weak-lined low-metallicity stars, as expected. Note that this scatter includes a contribution from errors in both spectroscopic and photometric metallicities. The median difference between spectroscopic and photometric metallicity as a function of spectroscopic metallicity and the $g-r$ color is shown in the right panel in fig. 6. The median difference is small for well-populated regions. However, the bias is photometric metallicity is not negligible in less-populated regions at the low and high ends of the spectroscopic metallicity range.

The distribution of calibration stars in the photometric metallicity vs. spectroscopic metallicity diagram looks similar to the bottom left panel in fig. A.2 from B10. Here we investigate variation of this distribution for four ranges of the $g-r$ color, as shown in fig. 7. The photometric metallicity saturates at the low-metallicity end at [Fe/H]~ -1.9 for the bluest stars, and at [Fe/H]~ -1.6 for the reddest stars. The photometric metallicity estimator is expected to show such saturation because the absorption of UV flux diminishes for very small optical depths. This effect begins to be noticeable at higher values of [Fe/H] for red stars because the SDSS sample is not deep enough to include a large fraction of red stars with low [Fe/H] (halo stars begin to dominate only for $r > 19$, and contribute only $\sim$1% of all stars in the solar neighborhood, Jurić et al. 2008).

Similarly, due to the distribution of calibration stars in the color-metallicity space, the photometric metallicity bias at the high-metallicity end for blue stars is 0.2 dex at [Fe/H]~ -0.5, and increases towards higher metallicity. The reason here is that there are not enough blue high-metallicity disk stars to constrain the fits (due to their redder turn-off

$g - r$ color than for halo stars). For the reddest stars, the photometric metallicity bias at [Fe/H]=0 is about 0.1 dex, which represents a significant improvement compared to 0.3 dex bias for the method from B10.

We have also tested the performance of the new method at the high-metallicity end using globular clusters NGC 2420 and M67, with metallicities of -0.37 and 0.0, respectively. For the $0.2 < g - r < 0.6$ segments of cluster sequences based on the re-reduction of SDSS images by An et al. (2008), we obtain the median photometric metallicities of -0.45 and -0.19, respectively. We assumed that random $u - g$ errors are negligible; 0.01 mag errors would shift the results by $\sim$0.1 dex towards lower values. The root-mean-square scatter of photometric metallicity along the $g - r$ vs. $u - g$ loci is 0.08 and 0.05 dex, respectively. This small scatter shows that the iso-metallicity contours in the maps derived here are well aligned with the cluster sequences (see the dashed lines in fig. 5). The agreement between photometric and spectroscopic metallicities for these two clusters improves if one assumes a systematic error in $u - g$ color of 0.02 mag (which would be consistent with uncertainties in photometric zeropoint calibration and interstellar dust reddening correction; An et al. 2008). With this assumption, the median photometric metallicities become -0.41 and -0.11, with the scatter of only 0.03 and 0.04 dex, respectively. For the very metal-rich cluster NGC 6791, with [Fe/H]=0.40, we obtain photometric metallicity of 0.08 and 0.21, depending on whether we allow for a systematic error in $u - g$ color (the color sequence for NGC 6791 barely passes through the calibrated color range).

Last, but not least, we test whether the increasing systematic errors in photometric metallicity estimates towards the faint end are properly removed with the new method. Figure 8 shows spectroscopic metallicity for stars selected from narrow ranges of $u - g$ and $g - r$ colors, as a function of the apparent magnitude in the g band. It is an implication of I08 and B10 photometric metallicity methods that metallicity should not be correlated with magnitude because it depends only on $u - g$ and $g - r$ colors. On the contrary, the spectroscopic metallicity drops by as much as 0.4 dex between the bright and faint ends (a gradient of 0.1 dex mag^{-1}), as discovered by Lee et al. (2011). This gradient is essentially a manifestation of the bias discussed in § 2.3 (independent analysis demonstrates that the problem is not in spectroscopic values). As shown in the figure, the new method developed here properly accounts for this bias and produces the same metallicity gradient with respect to magnitude. Note that both I08 and B10 methods would produce the same value of photometric metallicity for all stars in this subsample because the $u - g$ and $g - r$ colors are essentially fixed.

Here add a test of mock sample generated with Mario's Galfast model.

3. DISCUSSION

We present a new calibration of SDSS photometric metallicity estimator, based on a spectroscopic sample of ∼95,000 F and G stars from SDSS Data Release 8. As discussed in § 2.2, the differences in spectroscopic [Fe/H] between Data Releases 7 and 8 are not large (of the order 0.1 dex). The application of polynomial expressions for estimating photometric metallicity from Bond et al. (2010) to DR8 catalogs will result in similar systematic errors. However, the resulting values will be biased due to the impact of $u - g$ measurement errors. The method developed here, and summarized in § 2.6, is superior because it accounts for this bias (see fig. 8). The new method supercedes previously published work by I08 and B10.

Even with the improved statistical treatment, there are pitfalls that should be remembered when applying this method and interpreting results. First, robust application is limited to the region of color-magnitude-error space calibrated with the training sample.

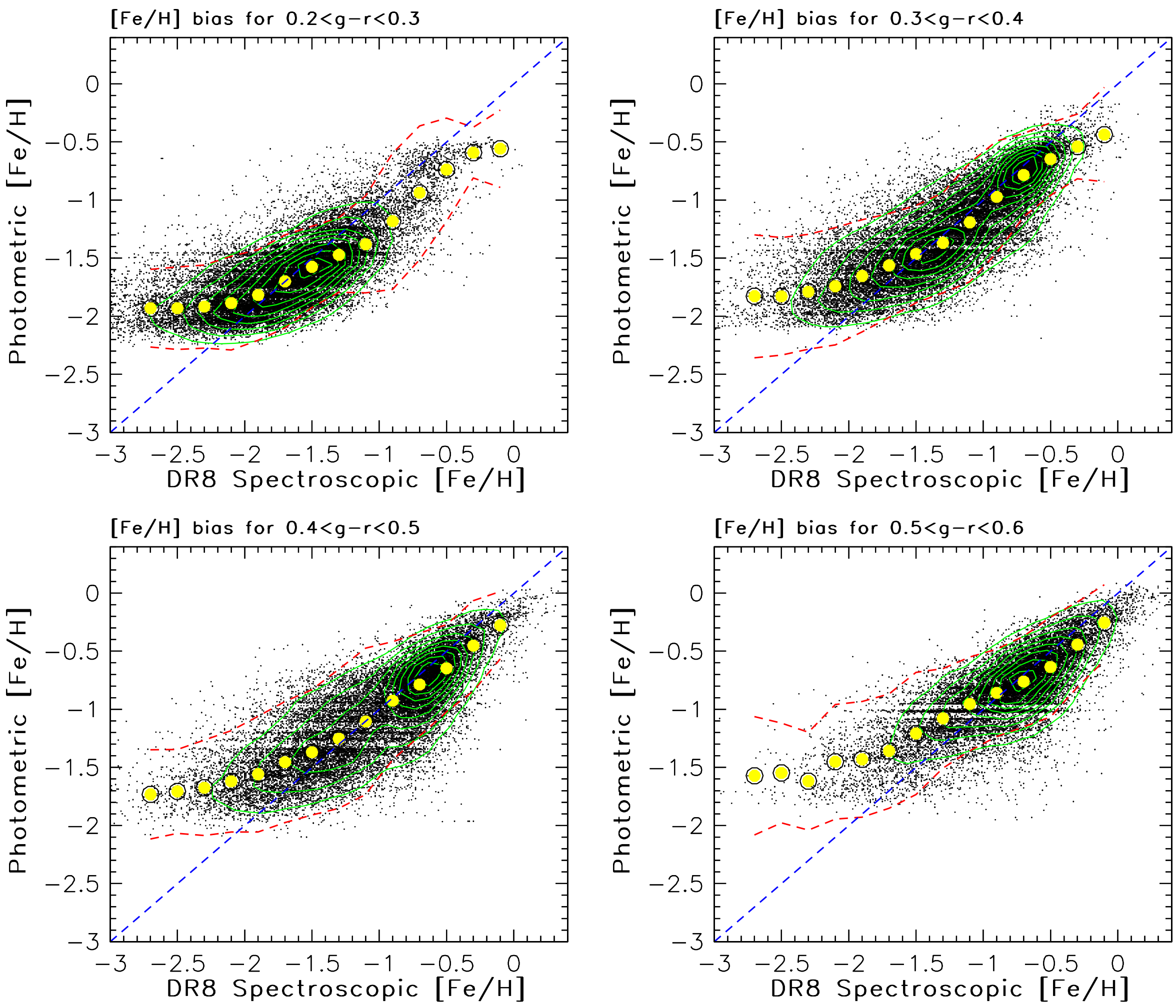

Fig. 7.— The panels show the photometric metallicity as a function of the spectroscopic metallicity, for four ranges of the $g - r$ color. Individual stars are shown by small dots, and the median values of the difference are shown by large circles. The distribution of stars is shown as linearly spaced contours. Note that the photometric metallicity saturates at the low-metallicity end at [Fe/H] $\sim$ 1.9 for blue stars, and at [Fe/H] $\sim$ 1.6 for red stars.

There is no guarantee that the linear approximation from eq. 4 will work for $u - g$ errors exceeding 0.1 mag. Second, much deeper samples than SDSS may be affected by true (or prior) [Fe/H] distribution, p([Fe/H]), in a quantitatively different way. Third, there are biases at the low-metallicity and high-metallicity ends, and they can exceed 0.2 dex

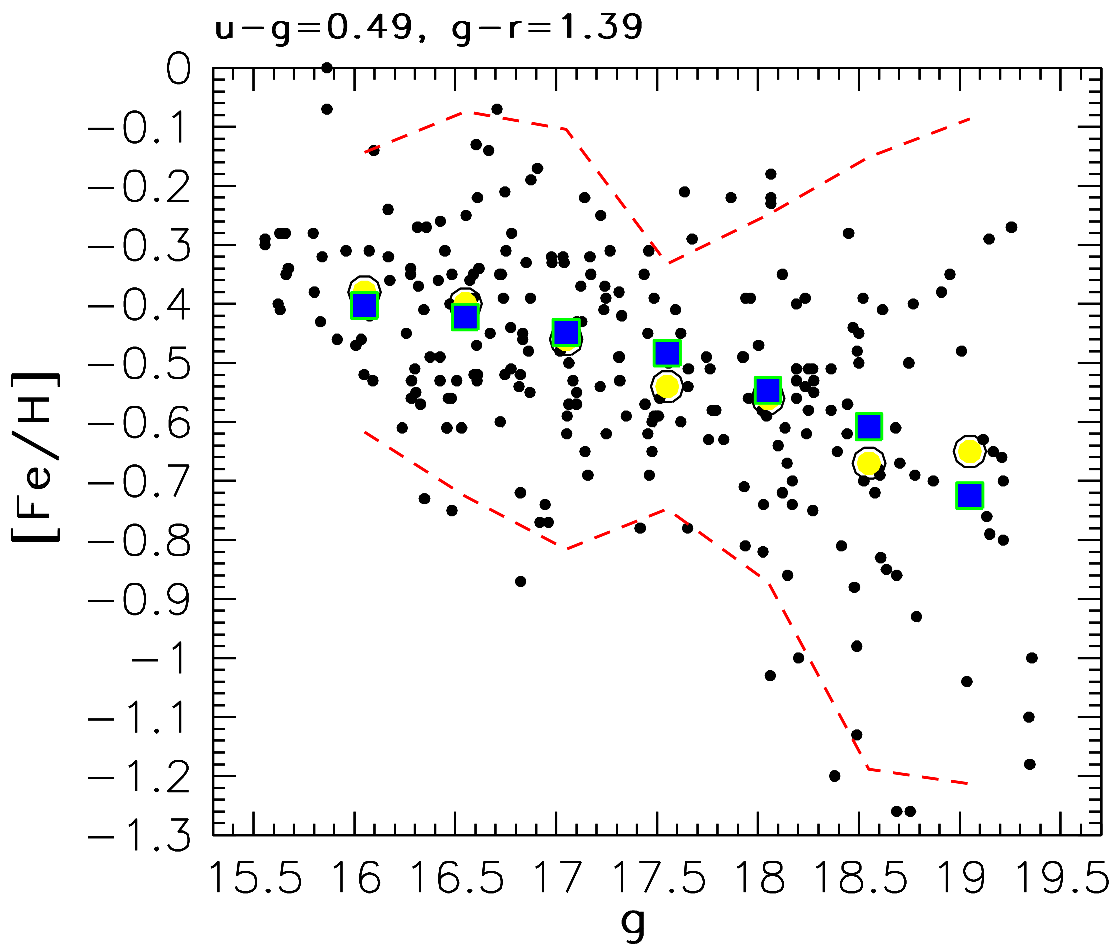

Fig. 8.— The small dots show spectroscopic metallicity for stars from the calibration sample with $0.48 < u-g < 0.50$ and $1.38 < g-r < 1.40$, as a function of apparent magnitude in the g band. The large circles are the median values in bins of g, and the two dashed lines show the $\pm 2\sigma$ envelope around the medians, where σ is the root-mean-square scatter estimated from the interquartile range. The squares are the median values of photometric metallicity for the same bins, and using the same stars.

in extreme cases. Lastly, the method is very sensitive to errors in the $u-g$ zeropoint calibration. The maps presented here are derived using SDSS photometry, and the $u-g$ and $g-r$ color calibration for any other sample should be verified to be on the same zeropoint scale (the SDSS $u - g$ color scale is offset by about 0.04 mag from AB magnitude scale, for details see Eisenstein et al. 2006). The same sensitivity to errors in $u - g$ measurements prevents this method from being useful when the interstellar dust reddening correction is uncertain.

Discuss Spagna and Lee et al. papers and test for v_ϕ vs. [Fe/H] correlation for thick disk stars.

4. Acknowledgments

Ž. Ivezić and S. Loebman acknowledge support by NSF grants AST-615991, AST-0707901, and AST-1008784 to the University of Washington, and by NSF grant AST-0551161 to LSST for design and development activity.

T.C. Beers, Y.S. Lee, and T. Sivarani acknowledge partial support from PHY 08-22648: Physics Frontier Center/Joint Institute for Nuclear Astrophysics (JINA), awarded by the U.S. National Science Foundation.

Funding for the SDSS and SDSS-II has been provided by the Alfred P. Sloan Foundation, the Participating Institutions, the National Science Foundation, the U.S. Department of Energy, the National Aeronautics and Space Administration, the Japanese Monbukagakusho, the Max Planck Society, and the Higher Education Funding Council for England. The SDSS Web Site is http://www.sdss.org/. The SDSS is managed by the Astrophysical Research Consortium for the Participating Institutions. The Participating Institutions are the American Museum of Natural History, Astrophysical Institute Potsdam, University of Basel, University of Cambridge, Case Western Reserve University, University of Chicago, Drexel University, Fermilab, the Institute for Advanced Study, the Japan Participation Group, Johns Hopkins University, the Joint Institute for Nuclear Astrophysics, the Kavli Institute for Particle Astrophysics and Cosmology, the Korean Scientist Group, the Chinese Academy of Sciences (LAMOST), Los Alamos National Laboratory, the Max-Planck-Institute for Astronomy (MPIA), the Max-Planck-Institute for Astrophysics (MPA), New Mexico State University, Ohio State University, University of Pittsburgh, University of Portsmouth, Princeton University, the United States Naval Observatory, and the University of Washington.

REFERENCES

An, D., et al. 2008, ApJS, 179, 326

Beers, T. C., et al. 2006, Memorie della Societa Astronomica Italiana, 77, 1171

Bond, N. A., et al. 2010, ApJ, 716, 1

Eisenstein, D. J., et al. 2006, ApJS, 167, 40

Flaugher, B. 2008, in A Decade of Dark Energy: Spring Symposium, Proceedings of the conferences held May 5-8, 2008 in Baltimore, Maryland. (USA). Edited by Norbert Pirzkal and Henry Ferguson. http://www.stsci.edu/institute/conference/spring2008

Freeman, K., & Bland-Hawthorn, J. 2002, ARA&A, 40, 487

Helmi, A. 2008, A&A Rev., 15, 145

Ivezić, Z., et al. 2008a, ArXiv e-prints

Ivezić, Ž., et al. 2008b, ApJ, 684, 287

Jurić, M., et al. 2008, ApJ, 673, 864

Kaiser, N., et al. 2002, in Society of Photo-Optical Instrumentation Engineers (SPIE) Conference Series, Vol. 4836, Society of Photo-Optical Instrumentation Engineers (SPIE) Conference Series, ed. J. A. Tyson & S. Wolff, 154

Lee, Y. S., et al. 2008a, AJ, 136, 2022

Lee, Y. S., et al. 2008b, AJ, 136, 2050

Lee, Y. S., et al. 2011, ArXiv e-prints

Majewski, S. R. 1993, ARA&A, 31, 575

Majewski, S. R. 2010, in IAU Symposium, Vol. 262, IAU Symposium, ed. G. Bruzual & S. Charlot, 99

Sandage, A. 1969, ApJ, 158, 1115

Wallerstein, G. 1962, ApJS, 6, 407

This manuscript was prepared with the AAS LaTeX macros v5.2.